Transport and Communications Science Journal, Vol. 77, Issue 4 (05/2026), 607-618

Transport and Communications Science Journal

DYNAMIC STABILITY ANALYSIS OF FUNCTIONALLY GRADED PLATE WITH VARIABLE THICKNESS

Nguyen Thao Hoa*

Engineers Department of the Staff Department, Military Region 2, Phu Tho, 35000, Vietnam

ARTICLE INFO

TYPE: Research Article
Received: 25/02/2026
Revised: 11/4/2026
Accepted: 03/5/2026
Published online: 15/5/2026
https://doi.org/10.47869/tcsj.77.4.20
* *Corresponding author*
Email: nguyenthaohoa@gmail.com

Abstract. Understanding the dynamic stability behaviour of functionally graded microstructures is of great importance for the development of advanced micro-electromechanical systems, aerospace components, and high-performance smart structures. Accurate prediction of instability regions and vibration characteristics can significantly improve structural reliability, safety, and lightweight design efficiency in modern engineering applications. This study presents an analytical method for analysing the dynamic stability of FG variable thickness microplate based on Mindlin plate theory, modified couple stress theory and the Bolotin method. The microplate thickness is assumed to vary along the length and width with a non-linear variation. The isogeometric analysis method is used to derive the pulse frequency and dynamic stability region of the plate under different boundary conditions. The accuracy of the model and calculation method is verified through numerical comparison with reliable publications. A set of numerical results is collected to evaluate the influence of input parameters; these results are crucial for the optimal calculation and design of variable thickness structures in practice.

Keywords: Dynamic stability, variable thickness, microplate, isogeometric method, functionally graded material, modified couple stress theory.

@ 2026 University of Transport and Communications

1. INTRODUCTION

The concept of functionally graded materials (FGMs) was initially introduced in Japan in 1984 as a new type of composite material with surface-to-surface variations in properties to carry out particular functions, such as eliminating stress concentrations and offering corrosion protection

from heat. Since the application of FGMs has lately spread to the realm of micro/nanotechnology, functionally graded (FGs) micro/nano beams and plates are commonly used in atomic force microscopy and micro and nanoelectromechanical systems (MEMS and NEMS). In these applications, empirically demonstrated size effects [1] would significantly influence the prospective uses of micro/nano FG beams and plates. Consequently, size effects must be considered when forecasting the static and dynamic responses of micro/nano functionally graded beams and plates. Traditional plate models grounded on continuum mechanics are incapable of predicting size effects due to the absence of intrinsic length scales. In recent years, various size-dependent plate models grounded in size-dependent continuum theories have been formulated, including non-local elasticity theory [2], strain gradient theory [3], couple stress theory [4], and its modified variant [5]. Numerous studies have examined microstructures of different thicknesses, such as [6], concentrating on addressing the static bending and natural vibration issues of the structure. Furthermore, Huong et al. [7] employed the IGA method to investigate the nonlinear free vibration of microplates with variable thickness and anisotropic mechanical properties, utilizing higher-order shear strain theory and modified couple stress theory. Anh et al. [8] identified the nonlinear free vibration characteristics of microplates with varied thicknesses composed of FG-GOEAM material through the application of the IGA method and MCST. Lawongkerd et al. [9] investigated the linear vibrational characteristics of multilayer microplate structures composed of graphene-reinforced functionally graded material, supported by a viscoelastic substrate and subjected to a thermal environment. Based on analytical methods, Tho and colleagues [10] analyzed the static bending of FG beams resting on a two-parameter elastic foundation. The vibration behavior of structures under explosive loads, especially plates with non-uniform thickness made of FGMs based on the finite element method, was discovered by Hung [11]. Most of these studies predominantly concentrate on assessing the static bending and vibrational properties of the structure, with a limited number examining its mechanical performance under dynamic loads. Forecasting the performance of structures subjected to dynamic loads is essential for the precise calculation and design of structures functioning in real-world conditions.

To analyze the dynamic stability response of microplates made of materials with variable mechanical properties and thickness that varies in both directions, this study suggests a combined model based on the Mindlin plate theory and the MSCT. This model combines the IGA method and the Bolotin method. The model is used to examine the impact of variables such as the thickness variation law, material qualities, and load type on the structure's dynamic stability response after being validated by comparison with trustworthy results in the literature. The findings of this study can help with the design, computation, and optimization of micro-electromechanical systems that support high-tech sectors like energy, semiconductor chips, sensors, and microprocessors.

2. MATHEMATICAL FOUNDATIONS AND MODELING

2.1. Geometric and material models

Examine a rectangle FG microplate with varied thickness, as depicted in Figure. 1. The geometrical dimensions of the FG microplate, including length L_x, width L_y, and thickness $h(x,y)$, are denoted as. The FG microplate consists of a material exhibiting diverse mechanical properties based on thickness, with the upper surface ($z = h/2$) composed wholly of ceramic and the lower surface ($z = -h/2$) composed entirely of metal. Throughout operation, the microplate experiences a load $P(\mathrm{t})$ applied in the neutral plane of the microplate. The law

governing the fluctuation in thickness of the microplate has a non-linear distribution in the horizontal plane, as illustrated below [7]:

$$h(x,y)=h_0\left\{1+\gamma_x\left(x/L_x\right)^{\lambda_x}\right\}\left\{1+\gamma_y\left(y/L_y\right)^{\lambda_y}\right\} \quad (1)$$

in this context, $\gamma_x,\gamma_y,\lambda_x,\lambda_y$ are the parameters that regulate the thickness of the microplate, whereas h_0 is the initial thickness of the plate structure. The mechanical properties of the plate material are delineated as follows [12]:

$$E(z)=E_m+(E_c-E_m)(0.5+z/h)^{p_z},\ \rho(z)=\rho_m+(\rho_c-\rho_m)(0.5+z/h)^{p_z} \quad (2)$$

where: $E(z),\rho(z)$ denote the elastic modulus and density of the plate material, respectively; the indices *m* and *c* signify the metal and ceramic components of the material, respectively; p_z denotes the material exponent factor.

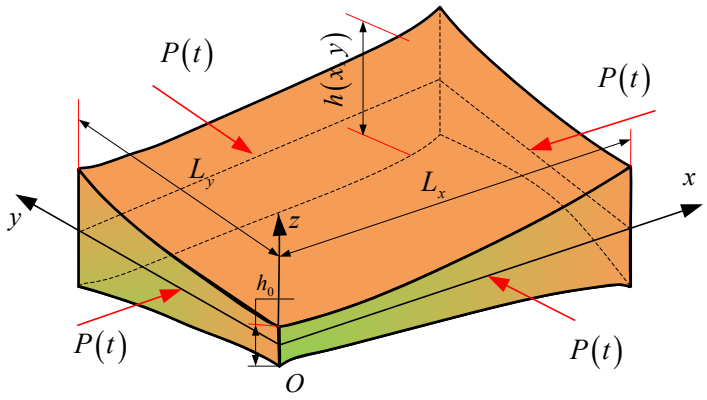

Figure 1. Mechanical microplate model with variable thickness.

2.2. Constitutive relationships

According to Mindlin's plate theory [13], the displacement at every point within the FG microplate with variable thickness is articulated as follows:

$$u(x,y,z)=u_0(x,y)+z\alpha_x(x,y),\ v(x,y,z)=v_0(x,y)+z\alpha_y(x,y),\ w(x,y,z)=w_0(x,y) \quad (3)$$

here: u_0,v_0,w_0 , α_x, α_y are the unknown displacement and rotational components.

The linear strain field of the variable thickness plate is described as below:

$$\boldsymbol{\varepsilon}_b=\boldsymbol{\varepsilon}_1+z\boldsymbol{\varepsilon}_2,\boldsymbol{\varepsilon}_s=\boldsymbol{\gamma}_0,\ \text{with:}\ \boldsymbol{\varepsilon}_1=\begin{Bmatrix}\dfrac{\partial u_0}{\partial x}\\ \dfrac{\partial v_0}{\partial y}\\ \dfrac{\partial u_0}{\partial y}+\dfrac{\partial v_0}{\partial x}\end{Bmatrix},\boldsymbol{\varepsilon}_2=\begin{Bmatrix}\dfrac{\partial \alpha_x}{\partial x}\\ \dfrac{\partial \alpha_y}{\partial y}\\ \dfrac{\partial \alpha_x}{\partial y}+\dfrac{\partial \alpha_y}{\partial x}\end{Bmatrix},\boldsymbol{\gamma}_0=\begin{Bmatrix}\dfrac{\partial w_0}{\partial x}+\alpha_x\\ \dfrac{\partial w_0}{\partial y}+\alpha_y\end{Bmatrix} \quad (4)$$

The curvature tensor components ϕ_{ij} are calculated using Yang's modified stress coupling theory [14].

$$\phi_b=\begin{Bmatrix}\phi_{xx}\\ \phi_{yy}\\ \phi_{zz}\\ \phi_{xy}\end{Bmatrix},\phi_s=\begin{Bmatrix}\phi_{xz}^1\\ \phi_{yz}^1\end{Bmatrix}-z\begin{Bmatrix}\phi_{xz}^2\\ \phi_{yz}^2\end{Bmatrix},\phi_{xx}=\frac{1}{2}\left(\frac{\partial^2 w_0}{\partial x\partial y}+\frac{\partial\alpha_y}{\partial x}\right),\phi_{yy}=-\frac{1}{2}\left(\frac{\partial^2 w_0}{\partial x\partial y}+\frac{\partial\alpha_x}{\partial y}\right), \tag{5a}$$

$$\begin{aligned}&\phi_{zz}=-\frac{1}{2}\left(\frac{\partial\alpha_y}{\partial x}-\frac{\partial\alpha_x}{\partial y}\right),\phi_{xy}=\frac{1}{4}\left(\frac{\partial^2 w_0}{\partial y^2}-\frac{\partial^2 w_0}{\partial x^2}+\frac{\partial\alpha_y}{\partial y}-\frac{\partial\alpha_x}{\partial x}\right),\phi_{yz}^1=\frac{1}{4}\left(\frac{\partial^2 v_0}{\partial x^2}-\frac{\partial^2 u_0}{\partial x\partial y}\right),\\ &\phi_{xz}^1=\frac{1}{4}\left(\frac{\partial^2 v_0}{\partial x\partial y}-\frac{\partial^2 u_0}{\partial y^2}\right),\phi_{yz}^2=\frac{1}{4}\left(\frac{\partial^2\alpha_x}{\partial y^2}-\frac{\partial^2\alpha_y}{\partial x\partial y}\right),\phi_{xz}^2=\frac{1}{4}\left(\frac{\partial^2\alpha_x}{\partial x\partial y}-\frac{\partial^2\alpha_y}{\partial x^2}\right)\end{aligned} \tag{5b}$$

The following is the weak form that describes the oscillation of a microplate of variable thickness, based on Hamilton's principle [15]:

$$\int_S\left(\delta\boldsymbol{\varepsilon}_b^T\boldsymbol{D}_b\boldsymbol{\varepsilon}_b+\delta\boldsymbol{\varepsilon}_s^T\boldsymbol{D}_s\boldsymbol{\varepsilon}_s+\delta\boldsymbol{\phi}_b^T\boldsymbol{D}_{mb}\boldsymbol{\phi}_b+\delta\boldsymbol{\phi}_s^T\boldsymbol{D}_{ms}\boldsymbol{\phi}_s\right)=\int_S\left(\delta\boldsymbol{\varepsilon}_w^T\boldsymbol{D}_w\boldsymbol{\varepsilon}_w\right)+\int_S\delta\boldsymbol{u}_b^T\boldsymbol{H}_b\ddot{\boldsymbol{u}}_b \tag{6}$$

where S is the area of the plate element.

$$\begin{aligned}&\boldsymbol{D}_b=\begin{bmatrix}\boldsymbol{A}&\boldsymbol{B}\\ \boldsymbol{B}&\boldsymbol{E}\end{bmatrix},\boldsymbol{D}_{ms}=\begin{bmatrix}\boldsymbol{P}&\boldsymbol{Q}\\ \boldsymbol{Q}&\boldsymbol{R}\end{bmatrix},\{\boldsymbol{A},\boldsymbol{B},\boldsymbol{E}\}=\int_{-h(x,y)/2}^{h(x,y)/2}\boldsymbol{Q}_b(1,z,z^2)\,\mathrm{d}z,\ \boldsymbol{D}_s=\frac{5}{6}\int_{-h(x,y)/2}^{h(x,y)/2}\boldsymbol{Q}_s\,\mathrm{d}z,\\ &\{\boldsymbol{P},\boldsymbol{Q},\boldsymbol{R}\}=\int_{-h(x,y)/2}^{h(x,y)/2}\boldsymbol{Q}_{ms}(1,z,z^2)\,\mathrm{d}z,\boldsymbol{D}_{mb}=\int_{-h(x,y)/2}^{h(x,y)/2}\boldsymbol{Q}_{mb}\,\mathrm{d}z,\boldsymbol{Q}_{ms}=\begin{bmatrix}2Gl^2&0\\ 0&2Gl^2\end{bmatrix},\\ &\boldsymbol{\varepsilon}_w^T=\begin{Bmatrix}\frac{\partial w_0}{\partial x}&\frac{\partial w_0}{\partial y}\end{Bmatrix},\boldsymbol{D}_w=\begin{bmatrix}P(t)&0\\ 0&P(t)\end{bmatrix},\end{aligned} \tag{7}$$

$$\boldsymbol{Q}_b=\begin{bmatrix}c_{11}&c_{12}&0\\ c_{12}&c_{22}&0\\ 0&0&c_{66}\end{bmatrix},\boldsymbol{Q}_{mb}=\begin{bmatrix}2Gl^2&0&0&0\\ 0&2Gl^2&0&0\\ 0&0&2Gl^2&0\\ 0&0&0&2Gl^2\end{bmatrix},\boldsymbol{Q}_b=\begin{bmatrix}c_{44}&0\\ 0&c_{55}\end{bmatrix}, \tag{8}$$

$$\boldsymbol{u}_b=\begin{Bmatrix}u_0\\ v_0\\ w_0\\ \alpha_x\\ \alpha_y\end{Bmatrix},\boldsymbol{H}_b=\begin{bmatrix}L_1&0&0&L_2&0\\ &L_1&0&0&L_2\\ &&L_1&0&0\\ &&&L_3&0\\ &&&&L_3\end{bmatrix},(L_1,L_2,L_3)=\int_{-h(x,y)/2}^{h(x,y)/2}(1,z,z^2)\,\mathrm{d}z \tag{9}$$

here: l called the length scale coefficient.

3. SOLUTION METHOD

3.1. The IGA method

Based on NURBS functions [14], displacement components $u_0, v_0, w_0, \alpha_x, \alpha_y$ of the FG microplate can be calculated as belows:

$$u_0 = \sum_{e=1}^{N_e} \begin{bmatrix} \boldsymbol{R}_e & 0 & 0 & 0 & 0 \end{bmatrix} \boldsymbol{d}_e = \sum_{e=1}^{N_e} \boldsymbol{\Gamma}_e^u \boldsymbol{d}_e, v_0 = \sum_{e=1}^{N_e} \begin{bmatrix} 0 & \boldsymbol{R}_e & 0 & 0 & 0 \end{bmatrix} \boldsymbol{d}_e = \sum_{e=1}^{N_e} \boldsymbol{\Gamma}_e^v \boldsymbol{d}_e \tag{10a}$$

$$w_0 = \sum_{e=1}^{N_e} \begin{bmatrix} 0 & 0 & \boldsymbol{R}_e & 0 & 0 \end{bmatrix} \boldsymbol{d}_e = \sum_{e=1}^{N_e} \boldsymbol{\Gamma}_e^w \boldsymbol{d}_e, \alpha_x = \sum_{e=1}^{N_e} \begin{bmatrix} 0 & 0 & 0 & \boldsymbol{R}_e & 0 \end{bmatrix} \boldsymbol{d}_e = \sum_{e=1}^{N_e} \boldsymbol{\Gamma}_e^x \boldsymbol{d}_e \tag{10b}$$

$$\alpha_y = \sum_{e=1}^{N_e} \begin{bmatrix} 0 & 0 & 0 & 0 & \boldsymbol{R}_e \end{bmatrix} \boldsymbol{d}_e = \sum_{e=1}^{N_e} \boldsymbol{\Gamma}_e^y \boldsymbol{d}_e \tag{10c}$$

where: $\boldsymbol{R}_e$ and $\boldsymbol{d}_e$ denote the unknown shape functions and displacement vectors at the control point *e*, respectively [14]; $N_e = (p+1)(q+1)$ is the number of control points per physical element. By inserting Eq. (10) into Eq. (6), the paper derives a comprehensive differential equation system that characterizes the oscillatory behaviour of the FG microplate with variable thickness as follows:

$$\boldsymbol{M}\ddot{\boldsymbol{d}} + \left(\boldsymbol{K} + P(\mathrm{t})\boldsymbol{K}_G\right)\boldsymbol{d} = \boldsymbol{0} \tag{11}$$

in which: $\boldsymbol{M} = \sum_{e=1}^{Nel} \boldsymbol{M}_e, \boldsymbol{K} = \sum_{e=1}^{Nel} \boldsymbol{K}_e, \boldsymbol{K}_G = \sum_{e=1}^{Nel} \boldsymbol{K}_{Ge}$ are the mass matrix, stiffness matrix and global geometric stiffness matrix of the structure respectively, their subcomponents are defined as below:

$$\boldsymbol{M}_e = \int_{S_e} \boldsymbol{N}^T \boldsymbol{H}_b \boldsymbol{N} dxdy, \boldsymbol{K}_{Ge} = \int_{S_e} \boldsymbol{B}_w^T \boldsymbol{D}_w \boldsymbol{B}_w dxdy, \boldsymbol{N} = \begin{bmatrix} \boldsymbol{\Gamma}_e^u & \boldsymbol{\Gamma}_e^v & \boldsymbol{\Gamma}_e^w & \boldsymbol{\Gamma}_e^x & \boldsymbol{\Gamma}_e^y \end{bmatrix}^T \tag{12}$$

$$\boldsymbol{K}_e = \int_{S_e} \left(\begin{Bmatrix} \boldsymbol{B}_1 \\ \boldsymbol{B}_2 \\ \boldsymbol{B}_s \end{Bmatrix}^T \begin{bmatrix} \boldsymbol{A} & \boldsymbol{B} & \boldsymbol{0} \\ \boldsymbol{B} & \boldsymbol{E} & \boldsymbol{0} \\ \boldsymbol{0} & \boldsymbol{0} & \boldsymbol{D}_s \end{bmatrix} \begin{Bmatrix} \boldsymbol{B}_1 \\ \boldsymbol{B}_2 \\ \boldsymbol{B}_s \end{Bmatrix} + \begin{Bmatrix} \boldsymbol{B}_{ms}^1 \\ \boldsymbol{B}_{ms}^2 \\ \boldsymbol{B}_{mb} \end{Bmatrix}^T \begin{bmatrix} \boldsymbol{P} & \boldsymbol{Q} & \boldsymbol{0} \\ \boldsymbol{Q} & \boldsymbol{R} & \boldsymbol{0} \\ \boldsymbol{0} & \boldsymbol{0} & \boldsymbol{D}_{mb} \end{bmatrix} \begin{Bmatrix} \boldsymbol{B}_{ms}^1 \\ \boldsymbol{B}_{ms}^2 \\ \boldsymbol{B}_{mb} \end{Bmatrix} \right) dxdy \tag{13}$$

$$\boldsymbol{B}_1 = \begin{bmatrix} \dfrac{\partial \boldsymbol{\Gamma}_e^u}{\partial x} \\ \dfrac{\partial \boldsymbol{\Gamma}_e^v}{\partial y} \\ \dfrac{\partial \boldsymbol{\Gamma}_e^u}{\partial y} + \dfrac{\partial \boldsymbol{\Gamma}_e^v}{\partial x} \end{bmatrix}, \boldsymbol{B}_2 = \begin{bmatrix} \dfrac{\partial \boldsymbol{\Gamma}_e^x}{\partial x} \\ \dfrac{\partial \boldsymbol{\Gamma}_e^y}{\partial y} \\ \dfrac{\partial \boldsymbol{\Gamma}_e^x}{\partial y} + \dfrac{\partial \boldsymbol{\Gamma}_e^y}{\partial x} \end{bmatrix}, \boldsymbol{B}_s = \begin{bmatrix} \boldsymbol{\Gamma}_e^x + \dfrac{\partial \boldsymbol{\Gamma}_e^w}{\partial x} \\ \boldsymbol{\Gamma}_e^y + \dfrac{\partial \boldsymbol{\Gamma}_e^w}{\partial y} \end{bmatrix}, \boldsymbol{B}_{ms}^1 = \frac{1}{4} \begin{bmatrix} \dfrac{\partial^2 \boldsymbol{\Gamma}_e^v}{\partial x \partial y} - \dfrac{\partial^2 \boldsymbol{\Gamma}_e^u}{\partial y^2} \\ \dfrac{\partial^2 \boldsymbol{\Gamma}_e^v}{\partial x^2} - \dfrac{\partial^2 \boldsymbol{\Gamma}_e^u}{\partial x \partial y} \end{bmatrix}, \tag{14}$$

$$\boldsymbol{B}_w^T = \left\{ \frac{\partial \boldsymbol{\Gamma}_e^w}{\partial x} \quad \frac{\partial \boldsymbol{\Gamma}_e^w}{\partial y} \right\}, \boldsymbol{B}_{ms}^2 = \frac{1}{4}\begin{bmatrix} \frac{\partial^2 \boldsymbol{\Gamma}_e^x}{\partial x \partial y} - \frac{\partial^2 \boldsymbol{\Gamma}_e^y}{\partial x^2} \\ \frac{\partial^2 \boldsymbol{\Gamma}_e^x}{\partial y^2} - \frac{\partial^2 \boldsymbol{\Gamma}_e^y}{\partial x \partial y} \end{bmatrix}, \boldsymbol{B}_{mb} = \begin{bmatrix} \frac{1}{2}\left(\frac{\partial^2 \boldsymbol{\Gamma}_e^w}{\partial x \partial y} + \frac{\partial \boldsymbol{\Gamma}_e^y}{\partial x} \right) \\ -\frac{1}{2}\left(\frac{\partial^2 \boldsymbol{\Gamma}_e^w}{\partial x \partial y} + \frac{\partial \boldsymbol{\Gamma}_e^x}{\partial y} \right) \\ -\frac{1}{2}\left(\frac{\partial \boldsymbol{\Gamma}_e^y}{\partial x} - \frac{\partial \boldsymbol{\Gamma}_e^x}{\partial y} \right) \\ \frac{1}{4}\left(\frac{\partial^2 \boldsymbol{\Gamma}_e^w}{\partial y^2} - \frac{\partial^2 \boldsymbol{\Gamma}_e^w}{\partial x^2} + \frac{\partial \boldsymbol{\Gamma}_e^y}{\partial y} - \frac{\partial \boldsymbol{\Gamma}_e^x}{\partial x} \right) \end{bmatrix} \tag{15}$$

here: T is the symbol for the transfer matrix.

3.2. Bolotin's method for dynamic buckling problem

According to Hoff [16], the static and dynamic components of the periodic compressive load are taken to be as follows:

$$P(\mathrm{t}) = P_s + P_d \cos\left(\boldsymbol{\omega t}\right) = P_{cr}\left(\eta + \psi \cos\left(\omega t\right)\right) \tag{16}$$

in which P_s is the static load and P_d denotes the vibration forced, P_{cr} is the static buckling load, ω is the pulsation frequency. Besides, η is the static load factor and ψ is the vibration load factor. Substituting Eq. (16) into Eq.(11), we have:

$$\boldsymbol{M}\ddot{\boldsymbol{d}} + \left\{ \boldsymbol{K} + P_{cr}\left(\eta + \boldsymbol{\psi} \cos\left(\boldsymbol{\omega t}\right)\right) \boldsymbol{K}_G \right\} \boldsymbol{d} = \boldsymbol{0} \tag{17}$$

The above equation is the equation of the Mathieu-Hill type, which establishes the dynamic instability response of plates subjected to the periodic compressive load. Bolotin's method is used to solve the dynamic unstable boundary. According to this approach, the displacement vector $\boldsymbol{d}$ may be given in the series with period $2T$ as follows [16]:

$$\boldsymbol{d} = \sum_{k=1,3,5\ldots}^{\infty} \left[a_k \sin\left(\frac{k\boldsymbol{\omega t}}{2} \right) + b_k \cos\left(\frac{k\boldsymbol{\omega t}}{2} \right) \right] \tag{18}$$

in which a_k and b_k are constant vectors. Based on Bolotin's theory [16] $k = 1$ can be approximated to gain the instability boundary. Substituting Eq. (18) into Eq. (17), the governing equation of the plates is rewritten as follows:

$$\boldsymbol{det}\left[\boldsymbol{K} + P_{cr}\left(\eta \pm \frac{\psi}{2} \right) \boldsymbol{K}_G - \frac{\omega^2}{4} \boldsymbol{M} \right] = 0 \tag{19}$$

Now, the critical static stability load can be determined, supposing $\psi = 0, \omega = 0$. The following boundary conditions are described and defined in the article: S stands for single support connection, and C for clamp connection.

4. SOME NUMERICAL RESULTS AND COMMENTS

4.1. Verify accuracy

Previous studies have shown that, for the rectangular microplate structure problem using the iso-geometric section method based on the NUBRS function, the calculation results achieve reliable convergence when the number of control points is 11×11 and the degree of the function is $p(q)$=4 [17]. Therefore, in this study, the number of control nodes is 11x11 and the element degree is $p(q)$=4 which are used for all the investigations in this study. Firstly, Table 1 presents a comparison of the non-dimensional natural frequencies $\Omega^* = \omega_1\sqrt{\rho_c L_x^4/\left(E_c h^2\right)}$ of the varying mechanical properties of the FG microplates. The thickness of the plates is specified as medium ($L_x/h=20$) and thin ($L_x/h=100$) with four values of the material length scale parameter l/h=0.2, 0.4, 0.8, 1.0. The findings provided by the paper are in full agreement with the results reported in [18] as seen in Table 1.

Table 1. Comparison of natural frequencies Ω^* of FG microplates.

		$p_z=0$		$p_z=1$		$p_z=10$	
L_x/h	l/h	[18]	paper	[18]	paper	[18]	paper
20	0.2	6.4027	6.4424	4.9568	4.9834	4.0323	4.0657
	0.4	7.6708	7.7081	6.0756	6.1016	4.7488	4.7755
	0.8	11.4108	11.4478	9.2887	9.3171	6.9013	6.9216
	1	13.5545	13.5934	11.1042	11.1352	8.1494	8.1691
100	0.2	6.4534	6.4551	4.9922	4.9940	4.0725	4.0751
	0.4	7.7217	7.7233	6.1126	6.1146	4.7840	4.7866
	0.8	11.4689	11.4704	9.3344	9.3370	6.9345	6.9375
	1	13.6186	13.6202	11.1560	11.1589	8.1846	8.1880

Next, a comparison of the critical buckling load values of isotropic plates with linearly varying thickness in the y-direction is presented in Table 2. The input parameters and exact results are published in the study [14]. From the data table, it can be seen that, with the change of the taper coefficient γ_y and the ratio L_x/L_y, the results proposed by the paper are in complete agreement with the results published in [14].

Table 2. The dimensionless buckling load values of a uniformly squeezed isotropic plate with changing thickness along the y-axis.

L_x/L_y	method	$\gamma_y=0.125$	$\gamma_y=0.25$	$\gamma_y=0.5$	$\gamma_y=1.0$
0.5	[14]	7.4621	8.7531	11.5687	18.1368
	paper	7.4625	8.7534	11.5691	18.1372
1.1	[14]	4.8363	5.7242	7.7729	12.9874
	paper	4.8366	5.7247	7.7732	12.9880
1.5	[14]	5.1931	6.1249	8.2311	13.4394
	paper	5.1935	6.1254	8.2321	13.4402

A study on dynamic stability characteristics of FG plates is examined. Material properties are given by: $E_c=14.4GPa, E_m=1.44GPa, \rho_c=12000kg/m^3, \rho_m=1200kg/m^3$, $v_c=v_m=0.38$,

$h=17.6\mu m, L_x=L_y=10h, k_z=1$. In Figure 2, the effect of the static force factor on the dynamic buckling behaviour of S-FGM plates and the influence of the dynamic force factor on the pulse factor are presented. When there is a change in the static load factor η, the results proposed in this paper are in complete agreement with the results published by Han et al. [19].

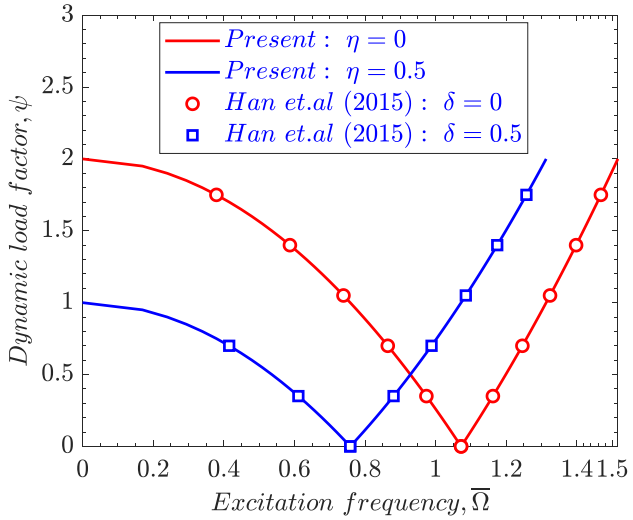

Figure 2. The effects of static load factor on the dynamic instability of S-FGM plate.

4.2. Results of the Survey

The microplate structure's input parameters are as follows in order to get the dynamic stability response results (some parameters will change during investigation; the remaining values remain unchanged): $h_0=17.6\mu m, L_x=10h_0, L_y=10h_0, l=0.3h_0, p_z=1, \gamma_x=0.15,$ $\gamma_y=0.25, \lambda_x=2.5, \lambda_y=1.5$. Variable mechanical properties materials made of metallic materials Al and ceramic materials ZrO_2 have mechanical properties [20] is $E_c=200GPa$, $v_c=0.3, \rho_c=3.0\,g/cm^3, E_m=70GPa, v_m=0.3, \rho_m=2.7\,g/cm^3$. The pulse frequency of the FG microplate is presented as numerical result plots as shown below:

$$\bar{\Omega}=\frac{\omega_1}{\pi^2}\sqrt{\frac{\rho_m L_y^4}{E_m h_0^2}} \tag{20}$$

First, the influence of the value p_z on the dynamic stability region response and pulse frequency $\bar{\Omega}$ of the FG microplate is described in Figure 3. It can be seen that as the value p_z increases, the stability region of the plate shifts to the left and the pulse frequency also decreases. This is explained by the fact that as the value p_z increases, the material phase of the FG microplate shifts from ceramic to a softer metal, and therefore the FG microplate becomes softer and more prone to instability. Furthermore, it can be seen that the CCCC boundary condition provides better stability than the SSSS boundary condition. Next, the effect of the length-scale parameter l on the stability region of the FG plate is described in Figure 4. It is easy to see that increasing the value will make the plate stiffer, due to the addition of strain energy. This directly causes the stability region of the structure to shift to the right with

increasing pulse frequency $\bar{\Omega}$. This is explained by the fact that, at the microscale, as the length-scale parameter l increases, the elastic strain energy of the structure increases, and therefore it becomes stiffer. However, when the size of the structure becomes macroscopic, this size effect will no longer have a significant impact and is often ignored. Finally, the influence of thickness rule control coefficients on the stability region of the FG microplate is described in Figure 5 and Figure 6. It can be seen that the taper coefficient γ_x, γ_y makes the structure thicker, which directly increases its stability, while an increase in the thickness rule control coefficient λ_x, λ_y makes the structure more prone to instability. Therefore, in practical design calculations, finding the specific thickness rule control is a prerequisite and crucial to the stability of the structure during operation.

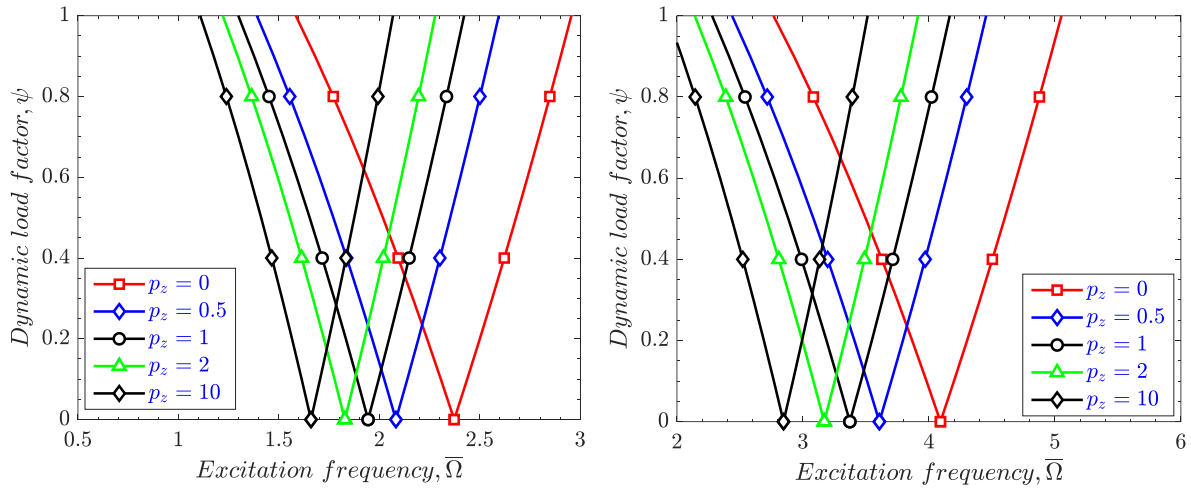

a) SSSS b) CCCC

Figure 3. The effect of grading index p_z on the stability region of the FG microplate.

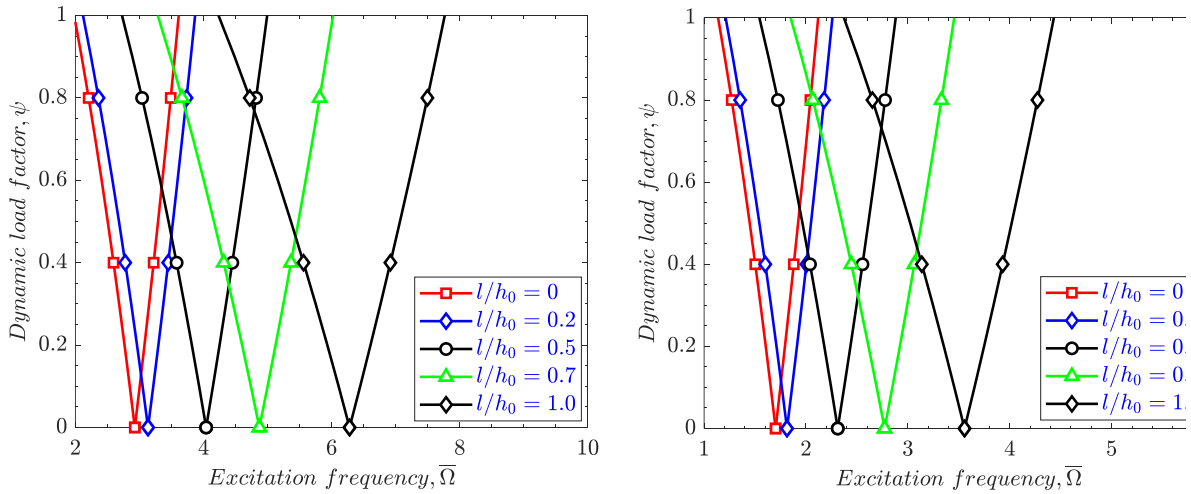

a) CCCC b) SSSS

Figure 4. The effect of length-scale parameter l on the stability region of the FG microplate.

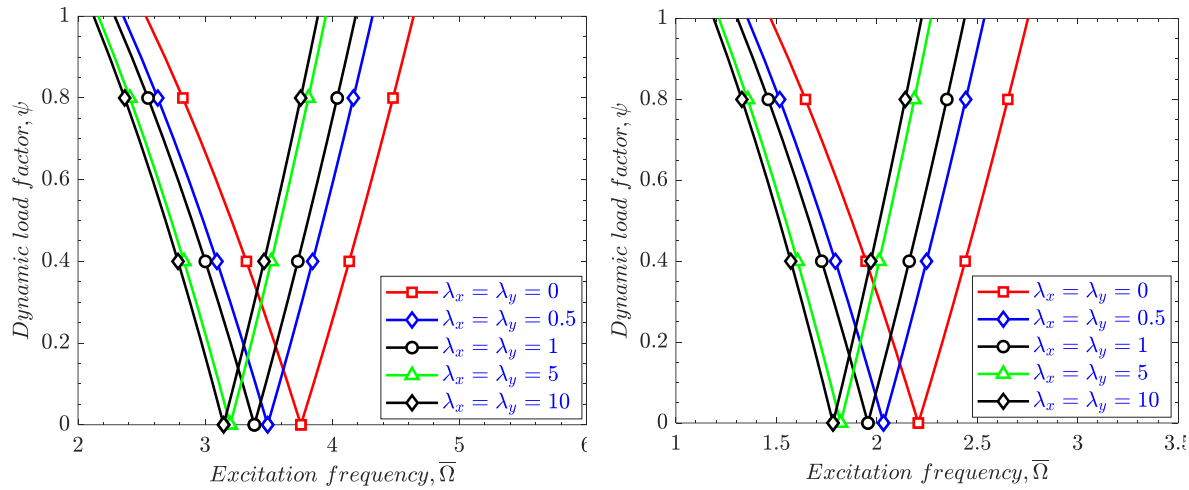

a) CCSS b) SSSS

Figure 5. Effect of thickness rule control coefficient λ_x, λ_y on the stability region of the FG microplate.

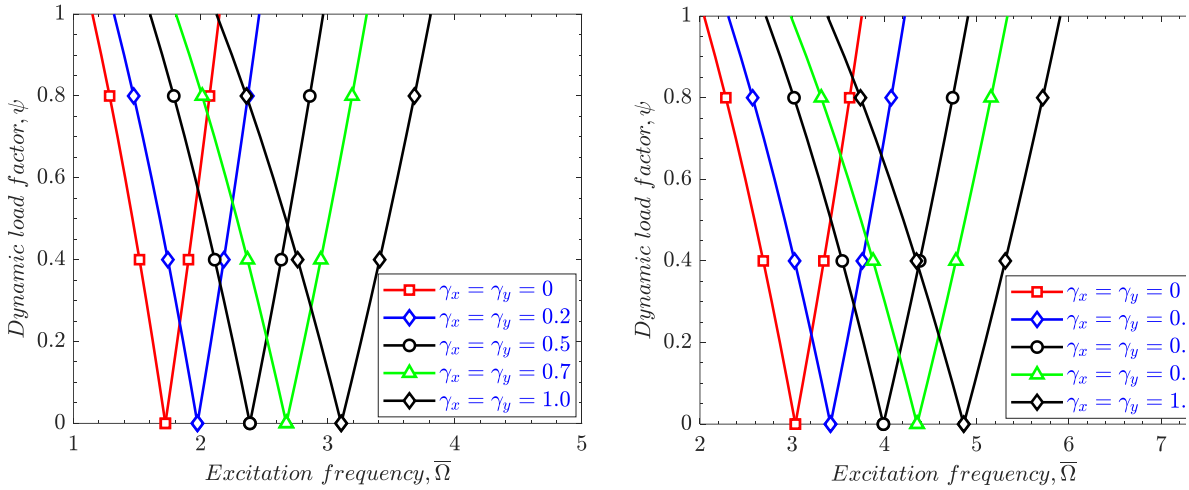

a) CCSS b) CCCC

Figure 6. Effect of taper coefficient γ_x, γ_y on the stability region of the FG microplate.

5. CONCLUSION

Based on the IGA method, modified stress couple theory, and first-order shear strain theory, this paper conducts a dynamic stability analysis of microplates made of materials with varying mechanical properties and a thickness that changes non-linearly in two directions in the horizontal plane. The paper established a computational program in MATLAB software and verified it through reliable numerical comparison. The study showed that the length-scale coefficient l greatly affects the stability of micrometer-sized structures, but this effect is ignored as the size grows to macro-scale. The stability region shifts to the left, and the pulse frequency decreases as the material volume coefficient p_z increases. Meanwhile, the taper coefficient γ_x, γ_y increases, making the microplate stiffer and thus increasing the microplate's

pulse frequency. Conversely, increasing the thickness rule control coefficient λ_x, λ_y causes the dynamic stability region to shift to the left and the pulse frequency to decrease. Furthermore, the pulse frequency and stability region results are highly dependent on various boundary conditions. These results can serve as useful references in the calculation and design of microelectromechanical structures, serving high-tech engineering fields such as semiconductors, chips, sensors, and biomedical engineering.

REFERENCES

[1]. N. A. Fleck, G. M. Muller, M. F. Ashby, J. W. Hutchinson, Strain gradient plasticity: Theory and experiment, Acta Metallurgica et Materialia, 42 (1994) 475-487. https://doi.org/10.1016/0956-7151(94)90502-9

[2]. A. C. Eringen, Nonlocal polar elastic continua, International Journal of Engineering Science, 10 (1972) 1-16. https://doi.org/10.1016/0020-7225(72)90070-5

[3]. D. C. C. Lam, F. Yang, A. C. M. Chong, J. Wang, P. Tong, Experiments and theory in strain gradient elasticity, Journal of the Mechanics and Physics of Solids, 51 (2003) 1477-1508. https://doi.org/10.1016/S0022-5096(03)00053-X

[4]. R. D. Mindlin, H. F. Tiersten, Effects of couple-stresses in linear elasticity, Archive for Rational Mechanics and Analysis, 11 (1962) 415-448. https://doi.org/10.1007/BF00253946

[5]. F. Yang, A. C. M. Chong, D. C. C. Lam, P. Tong, Couple stress based strain gradient theory for elasticity, International Journal of Solids and Structures, 39 (2002) 2731-2743. https://doi.org/10.1016/S0020-7683(02)00152-X

[6]. M. H. Shojaeefard, H. Saeidi Googarchin, M. Mahinzare, M. Ghadiri, Free vibration and critical angular velocity of a rotating variable thickness two-directional FG circular microplate, Microsystem Technologies, 24 (2018) 1525-1543. https://doi.org/10.1007/s00542-017-3557-8

[7]. T. H. N. Thi, V. K. Tran, V. K. Trai, L. Hoai, An IGA approach for linear and nonlinear free vibration of tri-directional functionally graded porous microplate in nonlinear high-temperature environment with nonlinear variable thickness, Thin-Walled Structures, 217 (2025) 113784. https://doi.org/10.1016/j.tws.2025.113784

[8]. V. N. Anh, T. V. Ke, N. T. T. Huong, N. T. Hue, P. H. Tu, Nonlinear free vibrations of functionally graded graphene origami-enabled auxetic metamaterial skew-microplates with variable thickness using isogeometric analysis, Defence Technology, 57 (2026) 85-108. https://doi.org/10.1016/j.dt.2025.09.024

[9]. J. Lawongkerd, P. R. Saffari, T. Jearsiripongkul, C. Thongchom, S. O. Ismail, P. R. Saffari, S. Keawsawasvong, Vibration characteristics of multilayer functionally graded microplates with variable thickness reinforced by graphene platelets resting on the viscoelastic medium under thermal effects, International Journal of Thermofluids, 22 (2024) 100611. https://doi.org/10.1016/j.ijft.2024.100611

[10]. T. Nguyen Chi, H. Vu Van, H. Le Hong, H. Nguyen Huu, T. Pham Duc, T. Dao Minh, Study of static bending of functionally graded beams using analytical method, Transport and Communications Science Journal, 76 (2025) 928-938. https://doi.org/10.47869/tcsj.76.7.1

[11]. N. V. Hung, The effect of blast loading on the forced vibration of functionally graded plates with nonuniform thickness, Transport and Communications Science Journal, 76 (2025) 1049-1063. https://doi.org/10.47869/tcsj.76.8.2

[12]. T. H. N. Thi, V. K. Tran, P. H. Tu, P. H. Thao, Finite element method for transient response of viscoelastic multi-directional FGP skew-nanoplate resting on visco-Pasternak foundation taking into account surface effect using nonlocal strain gradient theory, Acta Mechanica Sinica, 42 (2026) 524824. https://doi.org/10.1007/s10409-025-24824-x

[13]. T. T. T. Thuy, N. T. Anh, D. N. Mai, T. Van-Ke, Oscillation control of bio-inspired helicoid laminated composite shell integrated piezoelectric surface layer with initial geometrical imperfection, International Journal of Mechanics and Materials in Design, 22 (2026) 25. https://doi.org/10.1007/s10999-025-09860-7

[14]. T. Banh-Thien, H. Dang-Trung, L. Le-Anh, V. Ho-Huu, T. Nguyen-Thoi, Buckling analysis of non-uniform thickness nanoplates in an elastic medium using the Isogeometric Analysis, Composite

Structures, 162 (2017) 182-193. https://doi.org/10.1016/j.compstruct.2016.11.092
[15]. Q. H. Pham, V. K. Tran, T. T. Tran, P. C. Nguyen, P. Malekzadeh, Dynamic instability of magnetically embedded functionally graded porous nanobeams using the strain gradient theory, Alexandria Engineering Journal, 61 (2022) 10025-10044. https://doi.org/10.1016/j.aej.2022.03.007
[16]. V. V. Bolotin, Dynamic Stability of Structures, in Nonlinear Stability of Structures, A. N. Kounadis, W. B. Krätzig, Eds., International Centre for Mechanical Sciences, 342, Springer, Vienna, (1995) 3-72. https://doi.org/10.1007/978-3-7091-4346-9_1
[17]. P. Phung-Van, M. Abdel-Wahab, K. M. Liew, S. P. A. Bordas, H. Nguyen-Xuan, Isogeometric analysis of functionally graded carbon nanotube-reinforced composite plates using higher-order shear deformation theory, Composite Structures, 123 (2015) 137-149. https://doi.org/10.1016/j.compstruct.2014.12.021
[18]. H. X. Nguyen, E. Atroshchenko, H. Nguyen-Xuan, T. P. Vo, Geometrically nonlinear isogeometric analysis of functionally graded microplates with the modified couple stress theory, Computers Structures, 193 (2017) 110-127. https://doi.org/10.1016/j.compstruc.2017.07.017
[19]. S. C. Han, W. T. Park, W. Y. Jung, A four-variable refined plate theory for dynamic stability analysis of S-FGM plates based on physical neutral surface, Composite Structures, 131 (2015) 1081-1089. https://doi.org/10.1016/j.compstruct.2015.06.025
[20]. T. T. Tran, V. K. Tran, Q. H. Pham, A. M. Zenkour, Extended four-unknown higher-order shear deformation nonlocal theory for bending, buckling and free vibration of functionally graded porous nanoshell resting on elastic foundation, Composite Structures, 264 (2021) 113737. https://doi.org/10.1016/j.compstruct.2021.113737